## Plant Physiology®

# A sorghum ascorbate peroxidase with four binding sites has activity against ascorbate and phenylpropanoids

Bixia Zhang (1), 1 Jacob A. Lewis (1), 1 Wilfred Vermerris (1), 2 Scott E. Sattler (1) 3 and ChulHee Kang (1), 1

- 1 Department of Chemistry, Washington State University, Pullman, Washington 99164, USA
- 2 Department of Microbiology & Cell Science, UF Genetics Institute, and Florida Center for Renewable Chemicals and Fuels, University of Florida, Gainesville, Florida 32610, USA
- 3 U.S. Department of Agriculture—Agricultural Research Service, Wheat, Sorghum and Forage Research Unit, Lincoln, Nebraska 68583, USA

W.V., S.S., and C.K. conceived and coordinated this study. B.Z. performed the biochemical/biophysical/enzyme kinetics, computational chemistry, and structure determination. J.A.L. contributed to HPLC assay and NMR study. B.Z., J.W., W.V., S.E.S., and C.K. contributed to data interpretation, the writing of this manuscript, and approved of all content contained herein.

The author responsible for distribution of materials integral to the findings presented in this article in accordance with the policy described in the Instructions for Authors (https://academic.oup.com/plphys/pages/General-Instructions) is: ChulHee Kang (chkang@wsu.edu).

#### **Abstract**

Research Article

In planta,  $H_2O_2$  is produced as a by-product of enzymatic reactions and during defense responses. Ascorbate peroxidase (APX) is a key enzyme involved in scavenging cytotoxic  $H_2O_2$ . Here, we report the crystal structure of cytosolic APX from sorghum (Sorghum bicolor) (Sobic.001G410200). While the overall structure of SbAPX was similar to that of other APXs, SbAPX uniquely displayed four bound ascorbates rather than one. In addition to the  $\gamma$ -heme pocket identified in other APXs, ascorbates were bound at the  $\delta$ -meso and two solvent-exposed pockets. Consistent with the presence of multiple binding sites, our results indicated that the  $H_2O_2$ -dependent oxidation of ascorbate displayed positive cooperativity. Bound ascorbate at two surface sites established an intricate proton network with ascorbate at the  $\gamma$ -heme edge and  $\delta$ -meso sites. Based on crystal structures, steady-state kinetics, and site-directed mutagenesis results, both ascorbate molecules at the  $\gamma$ -heme edge and the one at the surface are expected to participate in the oxidation reaction. We provide evidence that the  $H_2O_2$ -dependent oxidation of ascorbate by APX produces a C2-hydrated bicyclic hemiketal form of dehydroascorbic acid at the  $\gamma$ -heme edge, indicating two successive electron transfers from a single-bound ascorbate. In addition, the  $\delta$ -meso site was shared with several organic compounds, including p-coumaric acid and other phenylpropanoids, for the potential radicalization reaction. Site-directed mutagenesis of the critical residue at the  $\gamma$ -heme edge (R172A) only partially reduced polymerization activity. Thus, APX removes stress-generated  $H_2O_2$  with ascorbates, and also uses this same  $H_2O_2$  to potentially fortify cell walls via oxidative polymerization of phenylpropanoids in response to stress.

#### Introduction

Heme peroxidase (EC 1.11.1) is part of a large superfamily that catalyzes a series of H<sub>2</sub>O<sub>2</sub>-dependent oxidation reactions of a wide range of organic and inorganic substrates. The superfamily of non-animal peroxidases (PRXs) is divided into three major classes (Welinder, 1992). Class I PRXs are intracellular peroxidases, which include ascorbate peroxidase (APX), cytochrome *c* peroxidase (Ccp), and the bacterial/fungal catalase-peroxidases. In plants, they are typically located

in the chloroplasts, cytosol, mitochondria, and peroxisomes. Class II PRXs include the secreted extracellular fungal hemecontaining enzymes such as lignin peroxidases and manganese peroxidases. They are glycosylated enzymes with four conserved disulfide bridges, bound Ca<sup>2+</sup> ions, and a short carboxy-terminal domain of 40–60 residues (Kjalke et al., 1992; Welinder, 1992). Class III PRXs comprise all plant secretory peroxidases, including the well-investigated horseradish peroxidase (HRP). In the peroxidase database PeroxiBase

<sup>\*</sup>Author for correspondence: chkang@wsu.edu (C.H.K.)

(Fawal et al., 2012), there are 16,613 PRXs from 2,643 organisms. During plant growth, Class III PRXs play a dual role in both cell wall stiffening and loosening (Francoz et al., 2015). In the presence of H<sub>2</sub>O<sub>2</sub>, Class III PRXs and laccases catalyze the oxidation reaction of the monolignols to generate their radicals, leading to oxidative radical coupling and lignin polymerization (Harkin and Obst, 1973; Higuchi, 1985; Lee et al., 2013; Li et al., 2003; Marjamaa et al., 2009; Moural et al., 2017).

Despite a range in preferred substrates, the  $H_2O_2$ -dependent catalytic reactions of the peroxidases are accomplished with three common steps: (1) the enzyme is oxidized by  $H_2O_2$  and forms intermediate Compound I; (2) Compound I is reduced by a substrate forming Compound II, resulting in one-electron oxidized substrate; (3) Compound II is then reduced by a second substrate, forming a water molecule, and returning the enzyme to a resting state of ferric (Fe(III)) heme iron (Figure 1A). Compound I in Class I APXs exists as a ferryl (Fe((IV)) heme and a porphyrin  $\pi$ -cation radical and its Compound II contains only a ferryl oxo species (Kwon et al., 2016; Ledray et al., 2020).

One of the most important manifestations of both biotic and abiotic stresses in plants is the increased production of reactive oxygen species (ROS), such as the superoxide radical  $(\cdot O_2^-)$ , the hydroxyl radical  $(\cdot OH)$ , and hydrogen peroxide (H<sub>2</sub>O<sub>2</sub>), which are produced as by-products of enzymatic reactions in various cellular compartments, or accumulate to activate signaling pathways allowing the plants to respond to, for example, attack by pathogens (Van Breusegem and Dat, 2006). Accumulation of H<sub>2</sub>O<sub>2</sub> is highly toxic for the cell, as H<sub>2</sub>O<sub>2</sub> is the only ROS that can pass through biological membranes and invade other sub-cellular compartments (Pandey et al., 2017). Stress-generated  $H_2O_2$  disturbs the electron transport system and cellular respiration associated with photosynthesis (Charles and Halliwell, 1980; Kaiser, 1976). Ascorbate is a well-known antioxidant that can react spontaneously with superoxide and other ROS. However, its rate constant for H<sub>2</sub>O<sub>2</sub> is low under physiological conditions  $(2M^{-1}s^{-1})$  (Polle et al., 1995). Together with catalase, APX catalyzes the removal of H<sub>2</sub>O<sub>2</sub> using ascorbate as an electron donor. In plants, APXs are widely present in the cytosol, peroxisome, mitochondria, and chloroplast, where they play a critical role in maintaining cellular homeostasis by removing H<sub>2</sub>O<sub>2</sub> produced by photosynthetic electron transport and photorespiration (Pandey et al., 2017; Saxena et al., 2011). In Arabidopsis (Arabidopsis thaliana) and rice (Oryza sativa L.), an eight-member APX multigene family was reported to encode three cytosolic, three microsomal, and two chloroplastic enzymes (Mittler et al., 2004; Pandey et al., 2017; Teixeira et al., 2004), although more recently the Arabidopsis genome was shown to only harbor six APX genes (Lazzarotto et al., 2021; Wang et al., 2014). The genome of sorghum (Sorghum bicolor (L.) Moench) (Paterson et al., 2009) contains seven APX genes that appear to be expressed broadly in all tissues and developmental stages. The sorghum gene atlas (Makita et al., 2015; Shakoor et al., 2014) indicates that the corresponding gene is moderately expressed in

many tissues and organs of the plant under controlled conditions. Expression of this gene is upregulated  $\sim$ 2–2.5 fold under drought or UV-light exposure.

It has been generally accepted that APX produces two monodehydroascorbate (MDHA) radicals from one H<sub>2</sub>O<sub>2</sub> molecule through two successive single-electron transfers (Figure 1B). In both plant and animal tissues, MDHA radicals have been known to be converted to dehydroascorbic acid (DHA1) and reduced enzymatically to ascorbate by DHA reductase or nonenzymatically by glutathione (GSH) (Winkler et al., 1994). Dehydroascorbic acid (DHA1) is hydrated rapidly at the 2'-position due to its high nucleophilicity in aqueous solutions to form the hydrated form DHA2, which in turn forms bicyclic hemiketal (DHA3) (Figure 1B) under physiological conditions (Kurata and Nishikawa, 2000). Although little information is available about the physiological role and predominant form of DHA in vivo, it has been proposed that a balanced ratio between ascorbate and DHA is as critical as NAD(P)H/NAD(P)+ and GSH/GSSG (Carroll et al., 2016; Kurata and Nishikawa, 2000). APX can also catalyze the oxidation of a variety of aromatic compounds, including pyrogallol, guaiacol, p-cresol, o-dianisidine, 2,2'-azinobis (3-ethylbenzothiazoline-6-sulfonic acid) (ABTS), and several non-physiological substrates (Heering et al., 2001; Raven, 2000). Recently, a dual functionality of poplar (Populus tomentosa) mitochondrial APX (PtomtAPX) has been reported based on its ability to translocate to the cell wall for autonomous lignification (Zhang et al., 2022). In addition, APX was identified as displaying 4-coumarate-3-hydroxylase (C3H) activity in Arabidopsis and Brachypodium dystachion (Barros et al., 2019), which implied the existence of an alternative pathway, leading to the formation of caffeic acid, rather than 4-coumaroyl-CoA (see reviews by Vanholme et al. (2019) and Yao et al. (2021)). When the activity of this enzyme was downregulated through RNAi, plants were impaired in lignin deposition, but its bifunctionality made it challenging to determine whether the reduced lignin phenotype resulted from the reduced APX or C3H activity.

So far, three APXs from dicots have been structurally characterized: APX from pea (*Pisum sativum*, rpAPX) (Patterson and Poulos, 1995), soybean (*Glycine max*, rsAPX) (Sharp et al., 2003), and tobacco (*Nicotiana tabacum*) (Wada et al., 2003). Here, we report the comprehensive characterization of APX from the monocot sorghum (SbAPX) encoded by the gene *Sobic.001G410200*. This gene was selected based on phylogenetic analyses that showed that Sobic.001G410200 and *Brachypodium* APX/C3H (Bradi1g65820) are members of the same family of cytosolic ascorbate peroxidases in grasses (https://phytozome-next.jgi.doe.gov/report/family/5269/124569777), and it was considered the best candidate to be the ortholog of *Brachypodium APX/C3H*.

We present crystal structures, steady-state kinetics for H<sub>2</sub>O<sub>2</sub>/ascorbate, and substrate specificity on aromatic compounds in the monolignol pathway. Furthermore, we describe the ascorbate oxidation product, bicyclic hemiketal dehydroascorbic acid, bound in SbAPX.

Α

$$APX (Fe^{III}) + H_2O_2 = APX (Fe^{IV} \cdot +) + H_2O$$
**compound I** (1)

$$APX (Fe^{IV}) + HS = APX (Fe^{IV}) + S \cdot$$
**compound II** (2)

$$APX (Fe^{IV}) + HS = APX (Fe^{III}) + S \cdot + H_2O$$
 (3)

B

dehydroascorbic acid (DHA1)

Ascorbate

monodehydroascorbate (MDHA)

bicyclic hemiketal (DHA3)

**Figure 1** APX reaction mechanism. A, General reaction scheme of APX. B, Ascorbate oxidation in aqueous solution. The ascorbate is first oxidized to MDHA, followed by reaction of two molecules of monodehydroascorbate forming dehydroascorbic acid (DHA1). In aqueous solution, DHA1 is hydrated (DHA2) and forms bicyclic hemiketal (DHA3).

#### Results

#### Enzyme preparation and spectral properties

Recombinant SbAPX enzyme was purified from Escherichia coli cells containing an expression vector harboring the Sobic.001G410200 cDNA sequence with the sequence encoding an N-terminal 6×His-tag at its 5' end. During the purification, the His-tag was spontaneously cleaved, which could be due to a thrombin site between the His-tag and SbAPX. Pure SbAPX displayed a Soret band with a maximum at 404 nm, with Q bands at 507 and 540 nm (Figure 2), which indicated the ferric (Fe(III)) form of SbAPX. Upon the addition of H<sub>2</sub>O<sub>2</sub>, both Soret bands and Q bands of the SbAPX solution were shifted to a longer wavelength, and the extinction coefficient was changed for the Soret band. When 20-fold molar excess of H2O2 was added, the first quick scan showed a Soret maximum at 413 nm and Q bands at 530 and 560 nm, which indicated heme compound II formation (Kwon et al., 2016) (Figure 2). The Q band at 530 nm gradually shifted to 538 nm after 1 min. However, the other Q band at 560 nm and the Soret band at 413 nm remained unchanged. When 200-fold molar excess of  $H_2O_2$  was added, the Soret band shifted to 413 nm and the Q bands shifted to 540 and 575 nm (Figure 2). This was similar to the observation of the formation of non-catalytic compound III from compound II upon addition of excess  $H_2O_2$  (Kwon et al., 2016). When ascorbate and/or p-coumaric acid were added to ferric SbAPX, no obvious change of spectrum was observed, indicating no reaction without  $H_2O_2$ .

#### The oxidation reaction of SbAPX

We examined the conversion of the potential substrate *p*-coumaric acid (Barros et al., 2019) by supplying SbAPX with *p*-coumaric acid and H<sub>2</sub>O<sub>2</sub> in phosphate buffer (pH 7.5). The reaction instantly turned the initial colorless solution into a light-yellow color and yielded three distinct product peaks in the HPLC profile (Figure 3A). The first product peak followed a Michaelis–Menten type of substrate concentration-dependency. However, the other two product

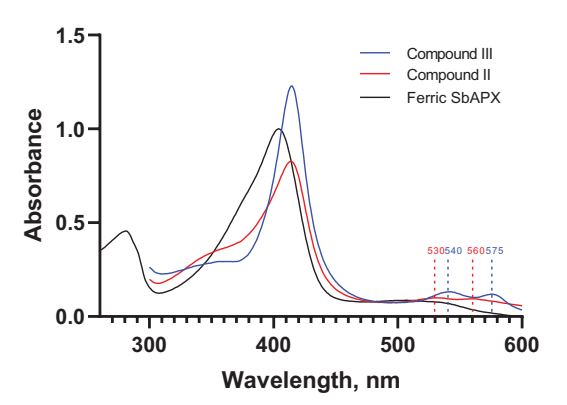


Figure 2 Spectra of purified SbAPX. The spectrum was recorded in 0.5 mL of Buffer C with  $5 \mu M$  of SbAPX at room temperature. A 20-fold (red, Compound II) or 200-fold molar excess of H<sub>2</sub>O<sub>2</sub> (blue, Compound III) was added to individual SbAPX solution and mixed prior to recording. The spectrum was normalized to have OD404 at resting ferric state (black) equal to one. The red and blue dotted lines indicate the wavelengths associated with the Q bands. The spectrum was collected using GENESYS<sup>TM</sup> 10S UV-Vis Spectrophotometer (Thermo Scientific, Waltham, MA) in the range of 260-700 nm. The first spectrum was recorded 10 s after mixing.

peaks displayed an almost linear, slightly sigmoidal trend, which was similar to the consumption of substrate, as shown in Figure 3, B and C. Mass spectrometry analyses determined that the parent ions for the peaks were two to six times the expected mass of p-coumaric acid (Supplemental Figure 1A), which suggests these products are due to radical polymerization catalyzed by APX. Other aromatic compounds were tested in the same buffer solution containing SbAPX and H<sub>2</sub>O<sub>2</sub>. Although cinnamic acid and tyrosine in the reaction mixture did not result in any product peaks, caffeic acid, ferulic acid, sinapic acid, coniferyl alcohol, and coniferyl aldehyde reaction mixtures produced product peaks (Figure 3D), indicating that this H<sub>2</sub>O<sub>2</sub>-dependent (and ascorbate-independent reaction) of SbAPX appears to be somewhat substrate specific.

Previously, hydroxylation of p-coumaric acid to caffeic acid was performed by supplying L-ascorbate and  $H_2O_2$  with either maize (Zea mays) extract or recombinant Brachypodium APX (or C3H) in phosphate buffer (pH 6) (Barros et al., 2019). Under the same condition with SbAPX (15 nM), caffeic acid production was confirmed by MALDI-MS (Supplemental Figure 1B) with a mass of 179.03471 at 1.7 ppm. The calculated mass of caffeic acid in negative mode is 179.0344. However, the control reaction without SbAPX showed a similar yield of caffeic acid compared to the enzymatic reaction. When the concentration of SbAPX was increased to 150 nM, the major products were the same as those p-coumarate polymers in the above reaction containing H<sub>2</sub>O<sub>2</sub> and p-coumarate in phosphate buffer (pH 7.5) and thus the dominant reaction was the polymerization instead of the hydroxylation (Figure 4). After 2 h incubation, enzymatic production of caffeic acid was only  $1.9 \pm 0.8\%$  of the yield in the reaction mixture without SbAPX, and most of the p-coumarate was polymerized. Overall, 3-hydroxylation of p-coumaric acid by SbAPX was not substantial at enzyme concentrations of either 15 nM or 150 nM.

HRP has been shown to hydroxylate p-coumaric acid in the presence of dihydroxyfumaric acid, but not NADH, H<sub>2</sub>O<sub>2</sub>, ascorbate, cysteine, or sulfite (Halliwell and Ahluwalia, 1976). We replicated this experiment with SbAPX, and our results indicated that SbAPX also catalyzed the hydroxylation of p-coumaric acid in the presence of dihydroxyfumaric acid. A control reaction was performed with the same solution without SbAPX. Purified product eluted from the C18 HPLC column was lyophilized and dissolved in 50% (v/v) acetonitrile for a MALDI/TOF experiment. Negative-mode MS was able to identify a compound with an m/z of 179.03392 at 2.7 ppm (Supplemental Figure 1C). Similar to the reaction containing p-coumarate, ascorbate, and  $H_2O_2$ , a nonenzymatic reaction was observed. During a 2-h reaction, approximately 50% of the caffeic acid was produced by the nonenzymatic reaction.

#### Steady-state kinetics of SbAPX for H<sub>2</sub>O<sub>2</sub>/ascorbate

Steady-state kinetics for the H<sub>2</sub>O<sub>2</sub>-dependent oxidation reaction of ascorbate were determined for SbAPX. The profile indicated an allosteric sigmoidal kinetic model (Copeland, 2000), instead of a Michaelis-Menten model. The fitting resulted in  $V_{max}$  of 14,626  $\pm$  1532 min<sup>-1</sup>, a Hill slope of 1.597  $\pm$ 0.2512, and  $K_{half}$  of 455.6  $\pm$  80.24  $\mu M.$  The Hill slope of larger than one indicated the positive cooperativity of multiple binding sites (Prinz, 2010) (Figure 5). Series of <sup>1</sup>H NMR spectra were measured upon the addition of H<sub>2</sub>O<sub>2</sub> and SbAPX to track the time progress of the reaction. When the reaction rate was adjusted by fixing the concentrations of SbAPX, H<sub>2</sub>O<sub>2</sub>, and ascorbate at 30 nM, 2 mM, 0.5 mM, we were able to observe time-dependence reduction of ascorbate and increase of the product. The product peaks were confirmed as a bicyclic hemiketal form (DHA3) through an <sup>1</sup>H NMR experiment (Figure 6).

#### Overall structure and heme environment of SbAPX

The apo-form SbAPX was crystallized in a P2<sub>1</sub>2<sub>1</sub>2<sub>1</sub> space group with one molecule in the asymmetric unit and its three-dimensional structure was determined at 1.3 Å resolution (PDBID: 8DJR). All the amino acid residues of the sequence were clearly verified from the high-resolution electron density map and the corresponding crystallographic statistics are listed in Supplemental Table S1. Analyzing the molecular interfaces of SbAPX in crystal lattices with PDBePISA server (Krissinel and Henrick, 2007), which evaluates interactions between neighboring monomers in the crystal lattices for the purpose of prediction biologically relevant oligomeric states, indicated that SbAPX likely exists as a monomer in solution (solvation free energy gain = -5.4 kcal  $mol^{-1}$  and interface complexation significance score = 0).

The apo-form structure showed what was presumably in the resting ferrous ion state (Fe(III)), a bound but noncoordinating water molecule was positioned distal to the heme at a distance of 2.2 Å from iron (Figure 7A), which

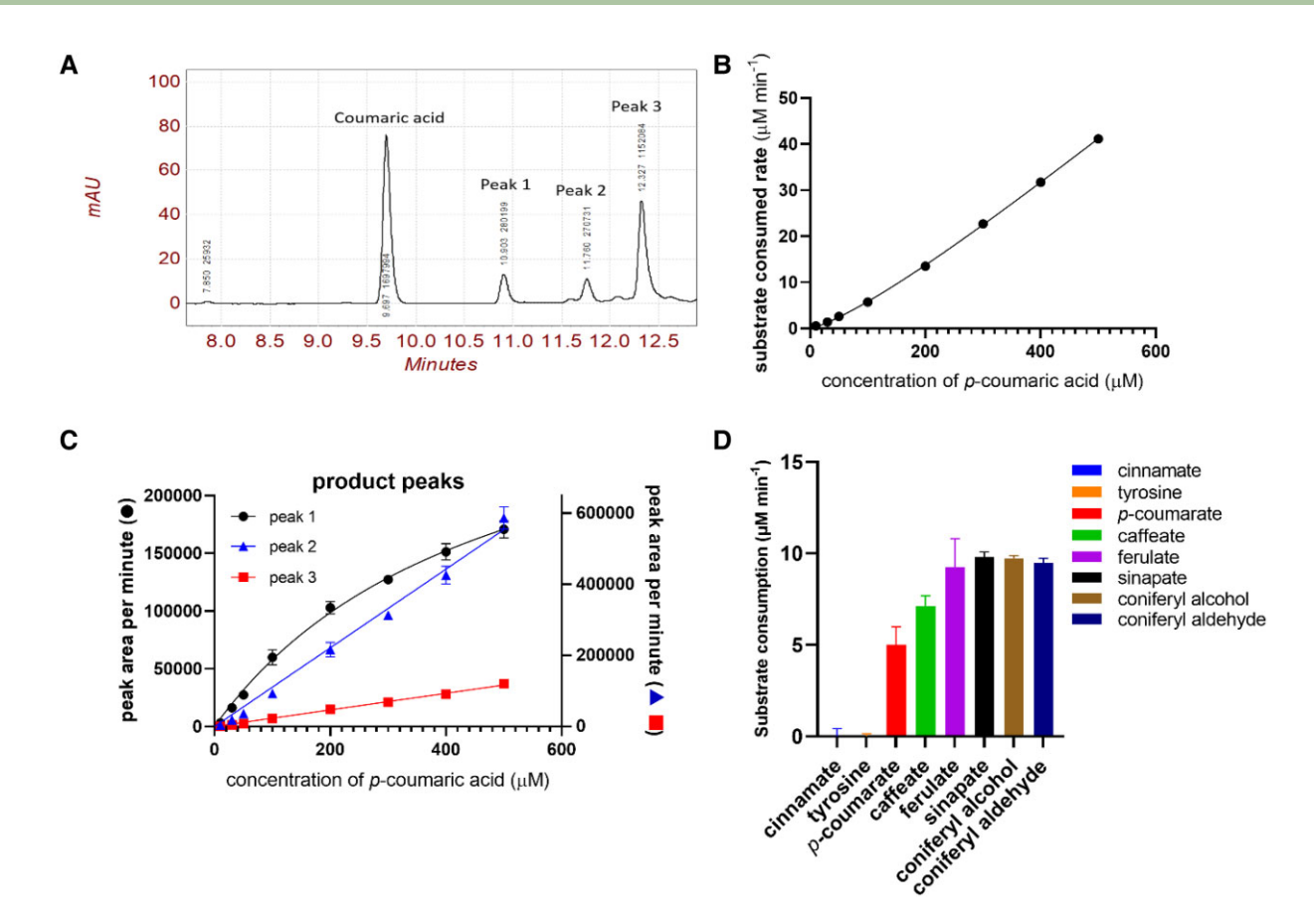


**Figure 3** SbAPX kinetic assay of  $H_2O_2$ -dependent oxidation of *p*-coumaric acid and ascorbate. A, HPLC chromatogram of the reaction products of the  $H_2O_2$ -dependent oxidation of *p*-coumaric acid. Peak 1 was mainly m/z 325.07, peak 2 was a mixture of m/z 651.15 and 977.22, and peak 3 was a mixture of m/z 325.07, 487.10, 651.15, and 977.22. B, The rate of *p*-coumaric acid consumption at different *p*-coumarate concentrations; the trend line was fitted with a sigmoidal equation. C, The rate of production of product peaks 1, 2, and 3 from panel A. The kinetic assay of SbAPX with *p*-coumarate was performed with 1 mM  $H_2O_2$  in 50 mM potassium phosphate buffer, pH 7.5. The concentration of *p*-coumarate varied from 10 to 500 μM and the concentration of SbAPX was 5 μM. The reactions were quenched after 10 min. The product peaks plots were fitted with Michaelis–Menten equation. D,  $H_2O_2$ -dependent oxidation of phenolic substrates. The bars indicate the average consumption of cinnamic acid, tyrosine, *p*-coumaric acid, caffeic acid, ferulic acid, sinapic acid, coniferyl alcohol, and coniferyl aldehyde (μM min<sup>-1</sup>). The data in figures B, C, and D experiments were based on triplicate analyses. Error bars indicate standard deviation.

was similar to the observed ferric heme species in rsAPX (Kwon et al., 2020; Moody and Raven, 2018). The  $N^{\epsilon}$  atom of His-42 on the distal side was hydrogen-bonded to a water molecule, which in turn hydrogen-bonded to the hemebound water molecule. In addition, this iron-bound water oxygen was 3.34 Å and 3.04 Å from the  $N^{\epsilon}$  atom of His-42 and Trp-41, respectively.  $N^{\delta}$  of the same His-42 is also hydrogen-bonded to the sidechain of Asn-71, thus, the position of the His-42 imidazole ring is expected to be fixed and the imidazole ring is expected to experience a positive electric field of the guanidium sidechain of Arg-38, which was at a distance of 4 Å. The hydrogen-bond network was further consolidated with surrounding water molecules, as three ordered water molecules reported in the distal pocket of the rsAPX structure (Sharp et al., 2003) were also found in our SbAPX structure. Heme iron of SbAPX was coordinated to the imidazole sidechain of His-163 from the proximal side and its propionyl groups were anchored through hydrogen bonds from the neighboring residues. The 7-propinate group

of the porphyrin ring was hydrogen-bonded with side chains of His-169 and Ser-173, and backbone amide of Ser-173. The 6-propinate group was hydrogen-bonded with backbone amide of Arg-167.

To identify the structural homologs in PBD, Dali search (Holm and Rosenstrom, 2010) was performed on the SbAPX structure. The result indicated that *G. max* cytosolic APX (PDBID: 1OAG) showed the highest Z-score of 45.4, followed by *P. sativum* cytosolic APX (PDBID: 1APX) with Z-score of 44.0, which, despite their lower Z-scores, were followed by *N. tabacum* chloroplastic APX (PDBID: 1IYN) with Z-score of 37.0, *Leishmania major* peroxidase (PDBID: 3RIW) with Z-score of 35.6, CcP from *Saccharomyces cerevisiae* (PDBID: 2BCN) with Z-score of 35.4, catalase-peroxidase from *Burkholderia pseudomallei* (PDBID: 5SYH) with Z-score of 29.4, and catalase-peroxidase from *Haloarcula marismortui* (PDBID: 1ITK) with Z-score of 28.5. Overall the 3D structure of APX from the monocot *S. bicolor* was similar to those from dicots (pea, soybean, and tobacco). The rmsd value of

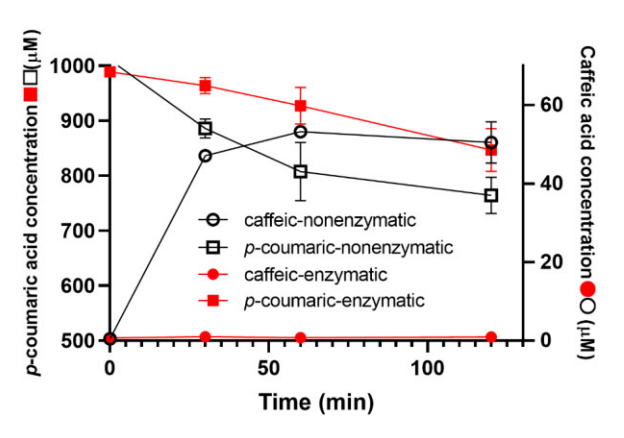


**Figure 4** Comparison of enzymatic and nonenzymetic *p*-coumarate-3-hydroxylation reaction. The concentrations of *p*-coumaric acid and caffeic acid were determined after quenching the reaction with glacial acetic acid at 0, 30, 60, and 120 min. The reaction mixture contained 75 mM potassium phosphate buffer (pH 6), 10 mM  $H_2O_2$ , 4 mM sodium ascorbate, 1 mM *p*-coumaric acid, and 150 nM SbAPX. The plots were based on triplicate analyses. Error bars indicate standard deviation.

SbAPX for rsAPX (PDBID: 1OAG), rpAPX (PDBID: 1APX), and tbAPX (1IYN) are 0.36 Å, 0.37 Å, and 0.72 Å, respectively. Specifically, tbAPX is a chloroplastic APX while others are cytosolic APXs, and its large structural difference is due to several insertions and deletions of amino acids. In those structurally characterized APXs, His-163 from ηC, Trp-179 from the loop between  $\beta B$  and  $\alpha G$ , and Asp-208 from  $\alpha H$  in the proximal heme pocket were present at the same position with similar sidechain orientations. On the distal side, Arg-38, Trp-41, and His-42 from αB are also conserved among those APXs. The corresponding residues of a short  $\beta$ -sheet that dicot APXs have adjacent to the 7-propionate of the heme were conserved as <sup>167</sup> Ala-Ala <sup>168</sup> and <sup>177</sup> Gly-Pro <sup>178</sup> in dicot cytosolic APX, but not among cytosolic APX from monocots such as sorghum and switchgrass (Pinicum virgatum). In addition, a high level of heterogeneity in amino acid sequence was observed in helices and loops located distal from the heme. The electron density of apo-form APX clearly showed a metal ion from the early stage of the refinement, which was located at the distal side and positioned 13 Å from heme iron. An Na<sup>+</sup> ion was placed, since this was the only cation present in our final purification step and crystallization procedures. The Na<sup>+</sup> ion was coordinated by the sidechains of Thr-164, Thr-180, Asn-182, Asp-187, and the backbone of Thr-164 and Asn-182 (Figure 8), all of which are conserved among APXs of known structures except for tbAPX. This position of the Na<sup>+</sup> ion is very close to the proximal Ca<sup>2+</sup> ion observed in many Class III peroxidases (Lee et al., 2013; Li et al., 2003; Marjamaa et al., 2009; Moural et al., 2017).

### SbAPX structure after a 1-minute soak in 1 mM ascorbate without $H_2O_2$

Electron density for a bound ascorbate was identified at the γ-heme edge position (PDBID: 8DJS) (Supplemental

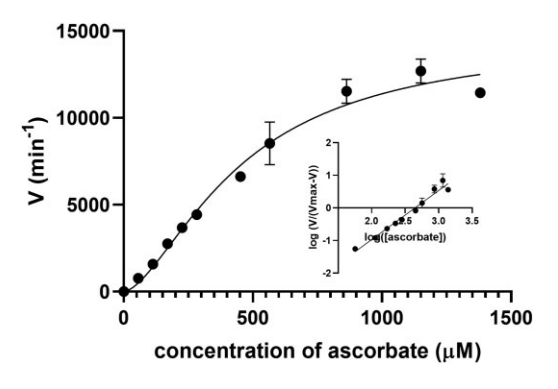


**Figure 5** Kinetic assay of  $H_2O_2$ -dependent oxidation of ascorbate by SbAPX. The reaction was performed with 1 mM  $H_2O_2$  in 50 mM potassium phosphate buffer, pH 7.0. The concentration of ascorbate varied from 10 to 1200  $\mu$ M and the concentration of SbAPX was 15 nM. Inset shows Hill plot fitted with linear regression; the slope indicated the Hill coefficient was equal to 1.5. Error bars indicate the standard deviation (n=3).

Figure 2). This pocket was surrounded by Cys-32, Pro-34, His-169, and Arg-172, all of which are highly conserved among the compared APX structures (Supplemental Figure 3). 2- and 3-hydroxyl groups of the ascorbate furan ring were hydrogenbonded to the 6-propionate group of the heme and the sidechain of Arg-172. In addition, the carbonyl oxygen of the furan ring of ascorbate was within a hydrogen-bond distance from the backbone nitrogen of Leu-35, and the 6-hydroxyl group of ascorbate was hydrogen-bonded to the backbone of Lys-30, which is similarly observed in rsAPX (PDBID: 1OAF) (Sharp et al., 2003, 2004). Compared to the apo-form, association of this ascorbate displaced five water molecules without any noticeable shift of surrounding side chains. This was somewhat different in the structure of rsAPX, where the side chain of Lys-30 swung to establish an extra hydrogen bond with bound ascorbate. In addition, at the  $\delta$ -meso side of the heme, there was an electron density resembling a glycerol molecule, likely from the cryoprotectant, which established a hydrogen-bond system with the sidechains of Trp-41 and His-42 and water molecules on the distal side of the heme. Especially, the O1 atom of glycerol was hydrogenbonded with a water molecule that, in turn, hydrogenbonded with the iron-bound H<sub>2</sub>O. The O3 atom of glycerol was indirectly hydrogen-bonded to the backbone carbonyl of Ala-70 and the backbone amide of Ala-134. Overall, bound glycerol in the  $\delta$ -meso site established a hydrogen-bond network with both nearby residues and water molecules and thus could be radicalized by SbAPX in the presence of  $H_2O_2$ .

### SbAPX structure after a 1-minute soak in 100 mM H<sub>2</sub>O<sub>2</sub> without ascorbate

SbAPX displayed a coordinated dioxygen species with its α-oxygen 1.83 Å from heme iron after a small dose of X-ray exposure ( $\sim$ 0.2 MGy), which was likely either Fe(III)-O-O- (anionic peroxide) or Fe(III)-O-OH (hydroperoxo) (PDBID: 8DJW) (Figure 7B). The N<sup>ε</sup> atoms of Trp-41

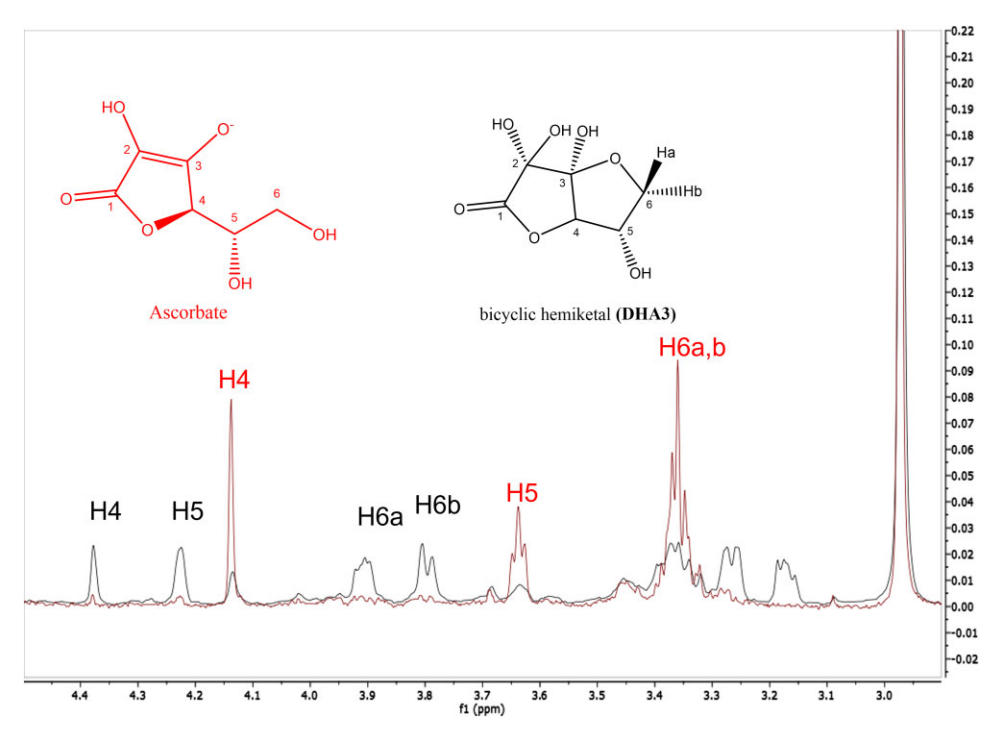


**Figure 6** NMR spectrum of  $H_2O_2$ -dependent oxidation of ascorbate with SbAPX. The peaks corresponding to hydrogens at C4, C5, and C6 were overlayed with those of ascorbate before (red spectrum) and after addition of  $H_2O_2$  and SbAPX (black spectrum).

(2.83 Å) and His-42 (3.33 Å) were hydrogen-bonded to the  $\alpha$ -oxygen of that dioxygen species. In addition, the  $\beta$ -oxygen of the dioxygen species was located within hydrogen bond distance from both N $^{\epsilon}$  atoms of Trp-41 (2.76 Å) and His-42 (2.71 Å). The N $^{\epsilon}$  atom of His-42 and the guanidium sidechain of Arg-38 were hydrogen-bonded to another water molecule in the distal pocket, which was in turn hydrogen-bonded to the  $\alpha$  and  $\beta$ -oxygen of the dioxygen species (Figure 7B).

With a higher dose of X-rays, we observed a mono-oxygen species with a distance of 1.82 Å to the heme iron (PDBID: 8DJX) (Figure 7C). According to the report of rsAPX crystal structures, compound II has a longer Fe-O distance compared to that in compound I (Moody and Raven, 2018). In addition, compound I of APX is unstable and rapidly degraded to compound II (Patterson et al., 1995). Thus, the heme iron of SbAPX exposed with a higher dose of X-ray (~1.3 MGy) should be a compound II, Fe(IV)-OH.

### SbAPX structure after a 10-minute soak in 1 mM ascorbate without $H_2O_2$

Clear electron density of four ascorbates bound to SbAPX was revealed (PDBID: 8DJT) (Figure 9, A and B), including the one at the above-mentioned  $\gamma$ -heme edge positions. In addition, another ascorbate molecule was identified at the  $\delta$ -meso position (Figure 9, A and B), where a glycerol molecule was observed in the structure of SbAPX following a 1-minute soak in ascorbate. Notably, the shape of the electron density indicated a mixture of glycerol and ascorbate.

The position of glycerol was the same as in the abovementioned 1-minute-soaked crystal, indicating some of the bound glycerol was replaced by ascorbate. Occupancy refinement indicated that approximately 60% and 40% were occupied by the ascorbate and glycerol molecules, respectively, in the crystal lattice. Compared to apo-form SbAPX, the association of ascorbate at the  $\delta$ -meso site displaced three water molecules. The 5- and 6-hydroxyl groups of ascorbate were hydrogen-bonded to  $N^{\epsilon}$  of His-42 and the backbone of Pro-132, respectively. The 6-hydroxyl group of the ascorbate at this position was also hydrogen-bonded to the heme ironcoordinated water or hydroxyl ion. However, 2- and 3-hydroxyl groups and the C1 carbonyl oxygen of ascorbate were solvent-exposed, which is an opposite orientation with respect to the heme for a proper oxidation reaction. Noticeably, there were two additional bound ascorbate molecules at the surface of SbAPX. Although the electron densities for those third and fourth ascorbates were well defined, their contour levels were slightly lower than those of the ascorbate molecules in the  $\delta$ -meso and  $\gamma$ -heme edge sites, indicating their weaker binding affinity (Figure 9B). The constituting residues in those third and fourth binding pockets are less conserved compared to those of the  $\delta$ -meso and y-heme edge sites. Only the 6-hydroxyl group of the third ascorbate molecule established a hydrogen-bond interaction with the sidechains of Asp-75 and Arg-79. The fourth ascorbate was anchored to the surface sidechain of Thr-135 and Ser-213. When compared with the apo-form SbAPX structure, the third ascorbate molecule displaced only one water molecule, and the fourth ascorbate displaced two water

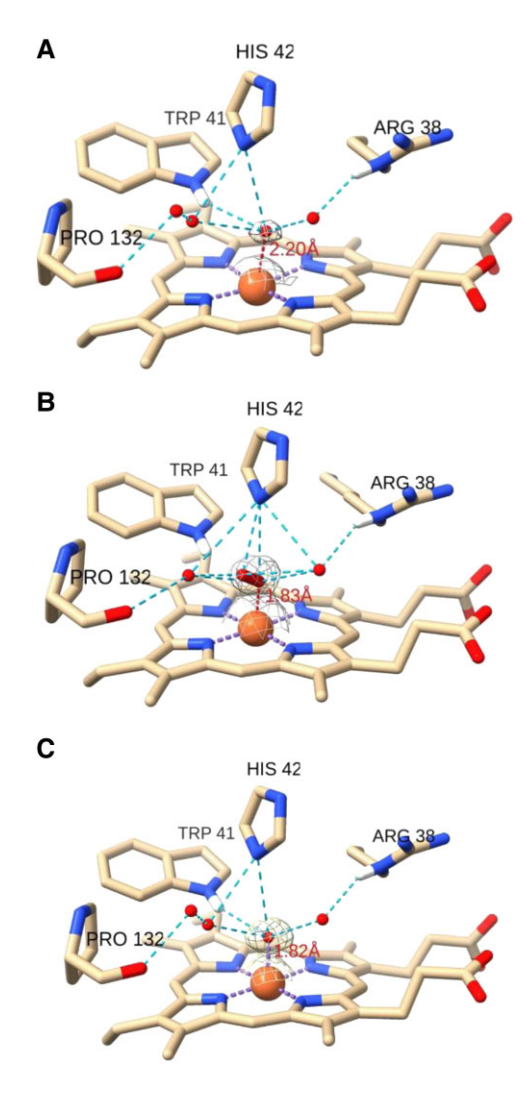


**Figure 7** Observation of heme compounds in SbAPX. Figures show the distal heme environment in (A) resting state (PDBID: 8DJR), (B) compound III (PDBID: 8DJW), and (C) compound II (PDBID: 8DJX). The electron density map at contour level 2 showed the distal water or oxygen species. This figure was produced using the Chimera package (UCSF, NIH P41 RR-01081).

molecules. Part of the bound ascorbates in the third and fourth sites was solvent-exposed and both ascorbates established an intricate hydrogen-bond network reaching the ascorbates at the  $\delta$ - and  $\gamma$ -sites (Figure 9C).

### SbAPX structure after soaking with both 50 mM H<sub>2</sub>O<sub>2</sub> and 50 mM ascorbate

The  $H_2O_2$ -dependent oxidation of ascorbate was monitored by soaking the apo-form SbAPX crystal in the mother liquor containing both ascorbate and  $H_2O_2$ . Upon this exposure, the crystal structure displayed a clear electron density for the hydrated bicyclic hemiketal form of DHA bound at its  $\gamma$ -heme edge position with an occupancy of 71% (PDBID: 8DJU), instead of the previously thought monodehydroascorbate or

dehydroascorbic acid (Figure 10). Compared to that of bound ascorbate at the  $\gamma$ -heme edge position, the original furan ring of bicyclic DHA was slightly reoriented, but 2- and 3-hydroxyl oxygens of the original furan ring maintained the same hydrogen bond distance from the propionyl group of the porphyrin ring. Two fused furan rings displayed C2'-exo puckering, indicating that resonating double bond character was eliminated upon cyclization. The 2- and 6-hydroxyl groups were directly hydrogen-bonded with the guanidinium sidechain of Arg-172, and the oxygen of the newly formed furan ring was hydrogen-bonded to the sidechain of Arg-167 through a water molecule. The carbonyl group on C1 also established a hydrogen bond with the backbone amide of Leu-35, and the 3-hydroxyl group was hydrogen-bonded with the sidechain of His-169.

#### Molecular docking

To further investigate the observed multiple sites of bound ascorbate and the binding preference for small molecules such as glycerol and other aromatic compounds, a corresponding molecular docking was performed with the structural coordinates of SbAPX. A global search indicated that the most energetically favorable binding site for ascorbate was the y-heme edge position (-4.8 kcal/mol), which is consistent with the position of ascorbate in the crystal structures of SbAPX (PDBID: 8DJS) and previously reported rsAPX. The next favorable site corresponded to the  $\delta$ -meso site (-4.7 kcal/mol). The glycerol molecule docked to the  $\delta$ -meso site exactly as observed in the crystal structure of SbAPX. When glycerol and salicylhydroxamic acid were docked to SbAPX, the  $\delta$ -meso site was consistently more energetically favorable than other sites. Thus, it is plausible that the  $\delta$ -meso site is the preferential binding site for various organic compounds and the y-heme edge is the primary site only for the ascorbate. All the phenylpropanoid intermediates of the monolignol pathway were docked to investigate the affinity of acids, alcohols, and aldehydes (Table 1). The preferred docked position of p-coumaric acid, caffeic acid, ferulic acid, and sinapic acid with SbAPX was again the  $\delta$ -meso site. Their phenolic rings faced toward the heme and the phenol oxygen of those acids established a hydrogen bond with Arg-38, and their propenyl oxygen also established a hydrogen bond with His-42. The carboxylate group of those compounds was hydrogen-bonded through water molecules with Ala-134 and Leu-131. The binding energy for p-coumaric acid, caffeic acid, ferulic acid, and sinapic acid were -5.6, -5.7, -6.1, and -6.2 kcal/mol, respectively (Table 1). Most of the alcohols and aldehydes showed the most negative free energy when their phenolic rings faced the heme group, although in the case of p-coumaryl aldehyde, caffeoyl alcohol, caffeoyl aldehyde, and coniferyl aldehyde, the most favorable orientation had the phenolic rings facing the solvent, while the phenolic ring facing the heme was the next most favorable orientation. When their phenolic rings were facing the heme group, these compounds all showed the same binding pattern as the aforementioned acids, interacting with both Arg-38 and His-42. In general, based on this

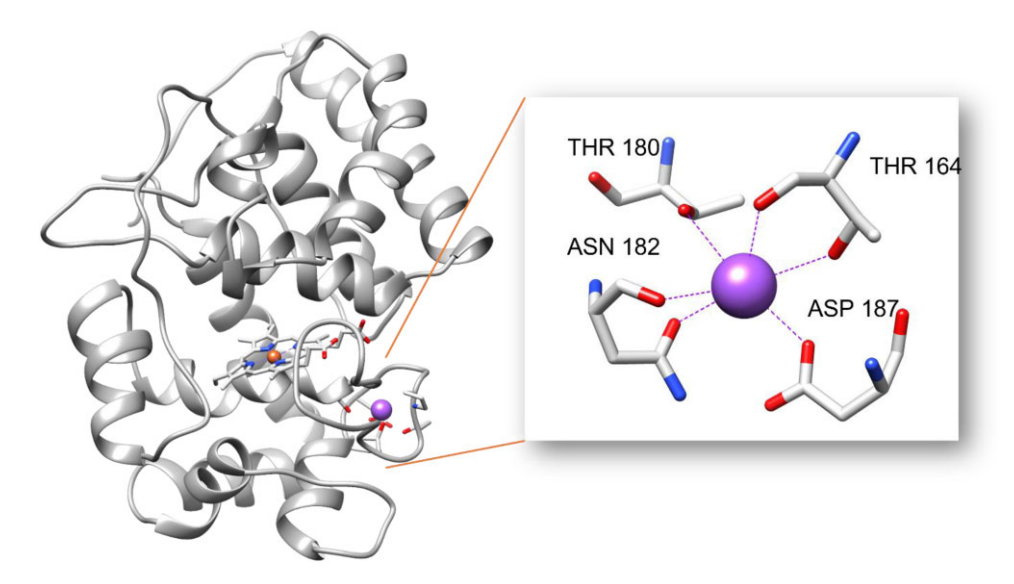


**Figure 8** Sodium ion on the proximal side of heme. An Na<sup>+</sup> ion was assigned, since there was no K<sup>+</sup> ion in either purification buffer or crystallization buffer. The corresponding position is very close to the proximal Ca<sup>2+</sup> ion observed in many Class III peroxidases (Lee et al., 2013; Li et al., 2003; Marjamaa et al., 2009; Moural et al., 2017). The Na<sup>+</sup> ion was coordinated by the sidechains of Thr-164, Thr-180, Asn-182, Asp-187, and the backbone of Thr-164 and Asn-182, all of which are conserved among APXs with known structures, except for tbAPX. This figure was produced using the Chimera package (UCSF, NIH P41 RR-01081).

analysis, the aldehydes were less preferred than acids and alcohols, and a greater degree of substitution on the phenolic ring decreased the binding energy.

#### Site-directed mutagenesis

As indicated by our molecular docking results and crystal structures, ascorbate oxidation might primarily occur at the χ-heme edge, whereas the H<sub>2</sub>O<sub>2</sub>-dependent radical polymerization reaction happens at the  $\delta$ -meso site. We conducted site-directed mutagenesis of the predicted key residues for ascorbate binding at the y-heme edge site (Arg-172) and deprotonation of H<sub>2</sub>O<sub>2</sub>/formation of Compound °C (Arg-38, Trp-41, and His-42). Thus, R172A was designed to eliminate ascorbate binding at the y-heme edge and to measure the polymerization activity. R38L, W41F, and H42A were designed to test the effect on both ascorbate oxidation and polymerization activity. The relative activity compared to the wild type is shown in Table 2. R172A showed only 3% ascorbate oxidation activity, consistent with what has been reported for rsAPX (Macdonald et al., 2006), but maintained ~40% of the activity of the polymerization reaction of p-coumarate. R38L maintained 48% of the ascorbate oxidation activity, while 15% of polymerization reaction activity remained, suggesting a marginal electrostatic effect. Both W41F and H42A displayed substantially lower activity for both ascorbate oxidation and polymerization.

#### **Discussion**

With the crystal structures of SbAPX at high resolution (up to 1.5 Å) in various conditions, we were able to observe substrate, product, heme compounds, and other bound ligands,

where the well-distinguished electron density peak illustrated the position of individual atoms. Uniquely, the structure of SbAPX indicated that there are four ascorbate-binding pockets including  $\gamma$ -meso and  $\delta$ -heme edge sites. In addition, SbAPX crystal in pH 7.5 buffer performed an H<sub>2</sub>O<sub>2</sub>-dependent ascorbate oxidation reaction and produced a C2-hydrated bicyclic hemiketal form of dehydroascorbic acid (DHA3) bound at its  $\gamma$ -heme edge.

Our enzymatic characterization of SbAPX indicated the existence of more than one kinetically competent ascorbate-binding site in SbAPX as predicted before (Lad et al., 2002). In addition, SbAPX catalyzed the radical polymerization reaction for *p*-coumaric acid, caffeic acid, ferulic acid sinapic acid, coniferyl alcohol, and coniferyl aldehyde (Figure 3D) and bound most phenylpropanoids intermediates in the monolignol pathway with substantial affinity (Table 2). In the presence of both ascorbate and H<sub>2</sub>O<sub>2</sub>, SbAPX catalyzed both the polymerization reaction and the 3-hydroxylation reaction of *p*-coumarate. SbAPX also produced caffeic acid in the presence of dihydroxyfumarate as reported previously for HRP (Halliwell, 1977). In both cases, however, a substantial amount of caffeic acid was produced in the same reaction mixture without SbAPX.

### Implication of bicyclic dehydroascorbic acid at the y-meso site

SbAPX crystals soaked in a buffer (pH 7.5) performed a  $H_2O_2$ -dependent ascorbate oxidation reaction and yielded, as product, the C2-hydrated bicyclic hemiketal form of dehydroascorbic acid (DHA3) that was still bound at its  $\gamma$ -heme edge. Therefore, in addition to the currently accepted view that APX activity reacts one  $H_2O_2$  molecule and two

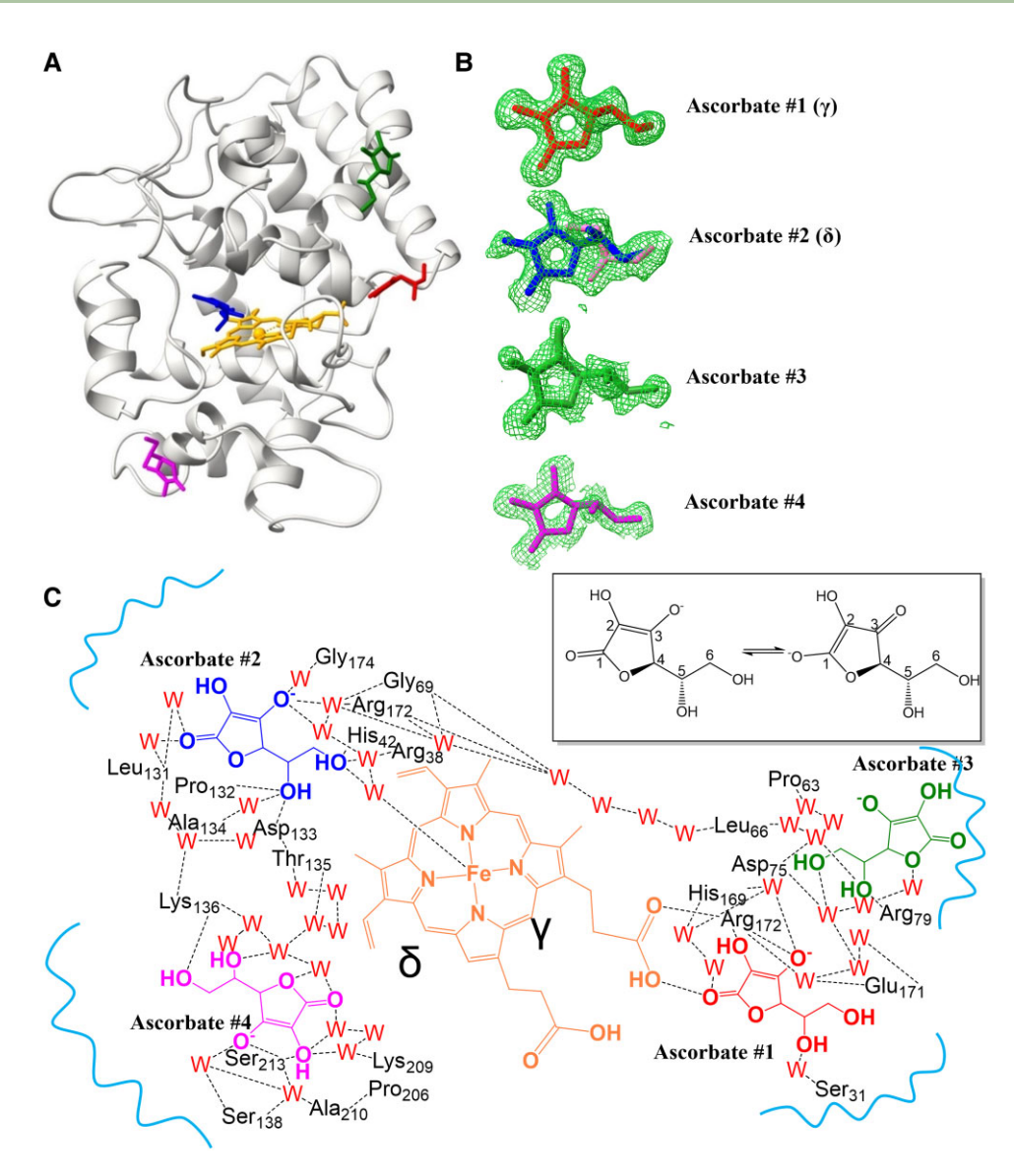


**Figure 9** Ascorbate binding sites in SbAPX. A, The four ascorbates in SbAPX are shown peripheral to the central heme group (PDBID: 8DJT). B, Electron densities of the four ascorbate molecules in SbAPX. The SA-omit maps (mF<sub>o</sub>-DF<sub>c</sub>) are shown for the four ascorbate molecules in the initial refinement at contour level 1.5. C, The observed hydrogen-bond network in which the four ascorbate molecules participate. Figures were produced using the Chimera package (UCSF, NIH P41 RR-01081).

ascorbate molecules to form two monodehydroascorbates (MDHA) (Miyake and Asada, 1992), SbAPX could also catalyze the transfer of two electrons from bound ascorbate through the propionyl group of porphyrin to produce a single DHA. The C2 carbonyl group is readily hydrated by the attack of nearby H<sub>2</sub>O, resulting in C-hydrate monocyclic DHA and an intramolecular cyclization reaction with a glycol moiety to produce a bicyclic hemiketal ring structure. This bicyclic form of oxidized ascorbate was identified in aqueous solutions decades ago (Pfeilsticker et al., 1975; Tolbert and Ward, 1982). Although bicyclic DHA has been thought not be predominant in the in vivo physiological range (Tolbert and Ward, 1982), an NMR experiment identified that it reached up to 60% of the total products of ascorbate oxidase (Kurata and Nishikawa, 2000). The remaining 40% was

2,3-diketo-l-gulonate and its degradation products suggesting that the predominant form of DHA in vivo could be the C2-hydrated bicyclic form (DHA3). The in vivo activity of those DHAs in an aqueous solution has been speculated to be different from that of ascorbate. The difference in their physicochemical characteristics, such as stability, compactness, and polarity, is considered to have a strong effect on their physiological behavior (Kurata and Nishikawa, 2000) and DHA has been proposed to be the preferred form for membrane transport (Vera et al., 1993; Washko et al., 1993).

### Implications of multiple ascorbate-binding sites *y-heme edge site*

Ascorbate molecules diffused into the crystals of SbAPX were associated preferentially with the y-heme edge site. Hydroxyl

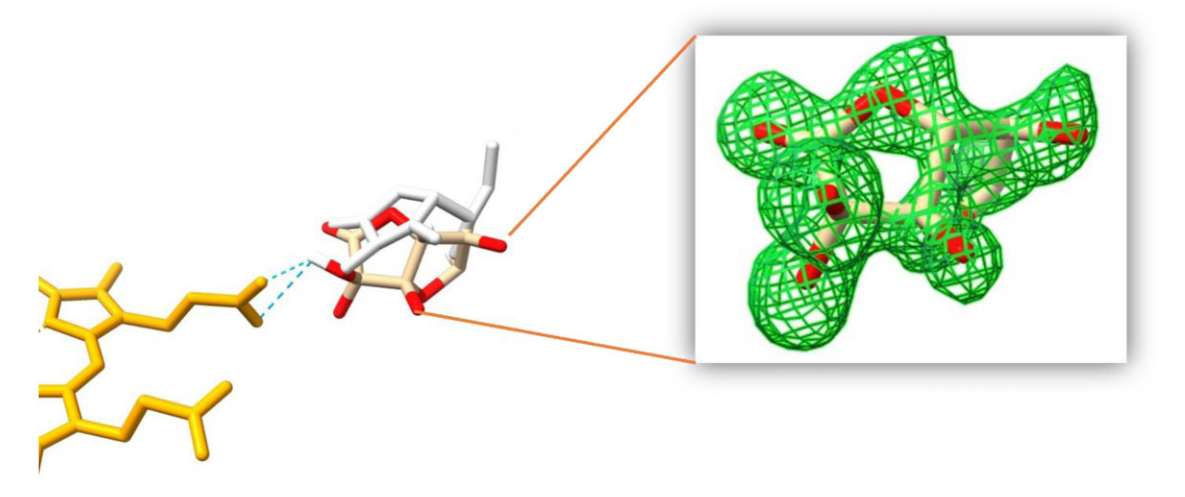


**Figure 10** The binding site of bicyclic dehydroascorbic acid (DHA3) with electron density shown. The position of the bicyclic hemiketal (DHA3; beige) (PDBID: 8DJU) was superimposed with the ascorbate at the  $\gamma$ -position (white). Propionate groups of heme were shown in yellow. The inset showed SA-omit map (mF<sub>0</sub>-DF<sub>c</sub>) of DHA3 at contour level 1.5. Figures were produced using the Chimera package (UCSF, NIH P41 RR-01081).

and carbonyl oxygens of the furan (or lactone) ring of ascorbate were hydrogen-bonded to the 6-propionate group of the heme porphyrin ring, the sidechain of Arg-172, and the backbone nitrogen of Leu-35. The ascorbate complex crystal structure of rsAPX (PDBID: 1OAF) also has its bound ascorbate at the y-heme edge site with the same conformation and orientation (Sharp et al., 2003, 2004). This y-heme edge is also observed in the manganese peroxidase/Mn<sup>2+</sup> complex, where the Mn<sup>2+</sup> was both coordinated with 6-propionate and nearby carboxylate oxygens of sidechains (Sundaramoorthy et al., 1994). The oxidation mechanism of the ascorbate molecule at this y-heme edge site has been proposed to follow the formation of a porphyrin  $\pi$ -cation radical in Compound I of APX and an electron is transferred from bound ascorbate via the propionyl group to the heme (Moody and Raven, 2018). In other Class III peroxidases, including HRP, the corresponding entrance for the ascorbate molecule is blocked by a salt bridge between a conserved arginine and glutamate/aspartate residues while the

Table 1 Molecular docking energy of phenylpropanoid intermediates of the monolignol pathway

Substrate	$\Delta G_{binding}$ (kcal mol $^{-1}$ )
<i>p</i> -Coumarate	-5.6
p-Coumaryl alcohol	-5.6
p-Coumaryl aldehyde	-5.3*
Caffeate	-5.7
Caffeyl alcohol	-5.9*
Caffeyl aldehyde	-5.5*
Sinapate	-6.2
Sinapyl alcohol	-6.3
Sinapyl aldehyde	-5.9
Ferulate	-6.1
Coniferyl alcohol	-6.0
Coniferyl aldehyde	-5.7*

All the energy values are for the result with phenolic rings facing the heme group. \*indicates the energy is the second lowest energy among all docked positions.

6-propionate group of the porphyrin ring was bridged by another conserved arginine residue. Therefore, the ascorbate molecule cannot enter in or bind to the  $\gamma$ -heme edge site of this class of peroxidases.

#### $\delta$ -meso site

SbAPX crystals soaked for 10 min in 1 mM ascorbate solution contained four ascorbate molecules including the y-heme edge site, the  $\delta$ -meso site, and the two surface sites. The ascorbate at the  $\delta$ -meso site was similarly located as the reported position of the bound salicylhydroxamic acid in rsAPX (PDBID: 1V0H) (Sharp et al., 2004), benzhydroxamic acid in the Arthromyces ramosus peroxidase (ARP) (PDBID: 1CK6), and ferulic acid in HRP (PDBID: 6ATJ) (Figure 11), and molecular docked phenylpropanoids in PvPRX (Lee et al., 2013; Li et al., 2003; Marjamaa et al., 2009; Moural et al., 2017). In addition, this second ascorbate was at the δ-heme edge was predicted previously based on NMR analysis (Hill et al., 1997) and the steady-state kinetics assays (Lad et al., 2002). However, an oxidizable hydroxyl group of the ascorbate at the  $\delta$ -meso position was not properly facing the heme-iron, preventing an effective electron transfer mediated by Trp-41 and His-42.

Our molecular docking approaches with SbAPX and p-coumarate also indicated binding at the  $\delta$ -meso position,

**Table 2** Ascorbate oxidation and *p*-coumarate polymerization activities of mutant versions of SbAPX relative to the wild-type version

Wild type/Mutant enzymes	Ascorbate oxidation (%)	Polymerization of <i>p</i> -coumarate (%)
WT	100	100
R38L	$48.2 \pm 4$	$15.3 \pm 2.3$
W41F	$2.3 \pm 0.3$	$9.3 \pm 0.2$
H42A	$2.4 \pm 0.4$	$4.6 \pm 1.5$
R172A	$2.8 \pm 0.5$	40.3 ± 12.1

which was consistent with the previous report on maize APX (Barros et al., 2019). The interacting residues, Arg-38, Trp-41, Pro-132, and Asp-133 are completely conserved among SbAPX and the other APX enzymes we compared (Supplemental Figure 3), as well CcP, which might result in a similar binding pattern of ligands at the  $\delta$ -meso site. However, in contrast to the ascorbate in the  $\delta$ -meso site of SbAPX, the bound salicylhydroxamic acid in the corresponding pocket of rsAPX is at a slightly different position establishing hydrogen bonds with a distal proline, tryptophan, arginine, or histidine where the N8 and O9 atoms of salicylhydroxamic acid were directly coordinated with heme iron. Figure 11 shows the superimposed salicylhydroxamic acid in rsAPX (PDBID: 1V0H), and glycerol and ascorbate at the δ-heme edge position of SbAPX, where the ligands in SbAPX did not directly coordinate to the heme iron. Those two ligands, ascorbate and glycerol, as well as p-coumarate to docked SbAPX, interacted with the heme iron via an ironcoordinating water molecule. The mouth area of  $\delta$ -meso site is larger than y-heme edge site in all structures of SbAPX, rsAPX, rpAPX, and tbAPX, which could allow diffusion of various aromatic compounds. In addition, the  $\delta$ -heme edge site is more hydrophobic than y-meso site, which could favor the binding of small aromatic acids (Supplemental Figure 4).

#### Two surface sites

Although the exact physiological relevance of these two additional surface sites in SbAPX is not clear and the affinities of these sites were slightly weaker than those of the y-heme edge and  $\delta$ -meso sites, it certainly allows association of two more ascorbate molecules. Both ascorbate molecules at those two sites were connected to ascorbate molecules at the  $\delta$ and y-meso positions through the hydrogen-bond network (Figure 9C). The interacting residues with those two ascorbates, Asp-75, Arg-79, Thr-135, and Ser-213, are conserved among SbAPX, rsAPX, and rpAPX (Supplemental Figure 3). Based on our crystal structures, steady-state kinetics, and sitedirected mutagenesis, it is tempting to propose that there are two catalytically competent ascorbate-binding sites, y-meso site and the closely hydrogen-bonded surface site (ascorbate #1 and #3 in Figure 9C). Considering the observed hydrogenbond network, the surface-bound ascorbate could synergistically contribute to the catalytic cycle for dismutation of harmful H<sub>2</sub>O<sub>2</sub>.

#### Catalytic reaction mechanism

In the first step of the catalytic reaction mechanism of SbAPX,  $H_2O_2$  displaces the water on the distal side of the Fe(III) heme in its resting state. Deprotonations of the  $\alpha$ -oxygen and  $\beta$ -oxygen of this  $H_2O_2$  by Trp-41 and His-42, respectively, results in an anionic peroxide species (Compound 0). The positive guanidinium side chain of Arg-38 could stabilize the resulting deprotonated negative  $\beta$ -oxygen of anionic peroxide and drive the reaction forward through electrostatic stabilization. In the second step, either Trp-41 or His-42 could donate a proton to the  $\beta$ -oxygen,

resulting in heterolytic cleavage of the hydroperoxyl O-O bond and the formation of H<sub>2</sub>O and the Fe(IV)-oxo heme  $\pi$ -cation radical (Compound I). Thus Trp-41 and His-42 conduct a general acid-base catalysis together with electrostatic catalysis of Arg-38, as supported by the substantially reduced activity of the corresponding mutant versions of SbAPX (Table 2). In the third step, the previously proposed direct electron transfer through the porphyrin  $\pi$ -system (Patterson et al., 1995; Sharp et al., 2004) seems plausible for the bound ascorbate molecule at the y-heme edge site, based on the distance and orientation of the hydroxyl group of the ascorbate with respect to porphyrin (Figure 9). Considering the form of product at the y-heme edge site, C2-hydrated bicyclic hemiketal DHA, two electrons have to be delivered from ascorbate to a heme-bound H<sub>2</sub>O<sub>2</sub> through the propionyl group of porphyrin, producing DHA via MDHA, and probably without dissociation from the χ-heme edge site. The C2 carbonyl group is readily hydrated by the attack of nearby H<sub>2</sub>O, resulting in C2-hydrate monocyclic DHA and an intramolecular cyclization reaction with a glycol moiety to produce a hemiketal ring structure. As in rsAPX (Sharp et al., 2003) and rpAPX (Patterson and Poulos, 1995), the mechanism proposed above based on the existence of a porphyrin  $\pi$ -cation radical is different from those of HRP and other Class III peroxidases, which involve a protein-based radical (Hiner et al., 2002; Jensen et al., 1998; Lee et al., 2013; Li et al., 2003; Marjamaa et al., 2009; Moural et al., 2017; Náray-Szabó, 1997; Pappa et al., 1996; Patterson and Poulos, 1995). In support of this mechanism for SbAPX, a metal ion was observed in the proximal pocket of SbAPX, which is coordinated by the sidechains of Thr-164, Thr-180, Asn-182, Asp-187, and the backbone of Thr-164 and Asn-182 (Figure 8). The corresponding residues are conserved among the APXs we compared (Supplemental Figure 3).

Considering the orientation of ascorbate at the  $\delta$ -meso site, the electron transfer efficiency should be much lower than that at the y-heme edge. The deprotonated ascorbate transfers an electron to the heme, resulting in the formation of a monodehydroascorbate radical that diffuses away, and Fe(IV)-oxo heme (compound II). Next, a second ascorbate binds to the enzyme. Upon binding, the ascorbate is deprotonated through a water-mediated proton shuttle, protonating the oxo ligand of the heme to form a Fe(IV)-hydroxo heme. The deprotonated ascorbate then transfers an electron to the heme, and Trp-41 or His-42 protonates the hydroxo ligand of the Fe(IV)-hydroxo heme, generating a second water molecule and the second monodehydroascorbate radical, which diffuses out of the pocket, thereby regenerating the resting-state APX. The electron transfer is plausible for the surface-bound ascorbate molecule (#3 in Figure 9), whose furan ring was establishing  $\pi$ -stacking with the guanidium sidechain of Arg-79 in addition to establishing hydrogen bonds with the hydroxyl groups. Thus, this position could facilitate an electron transfer to the y-heme edge ascorbate through the existing hydrogen-bond network

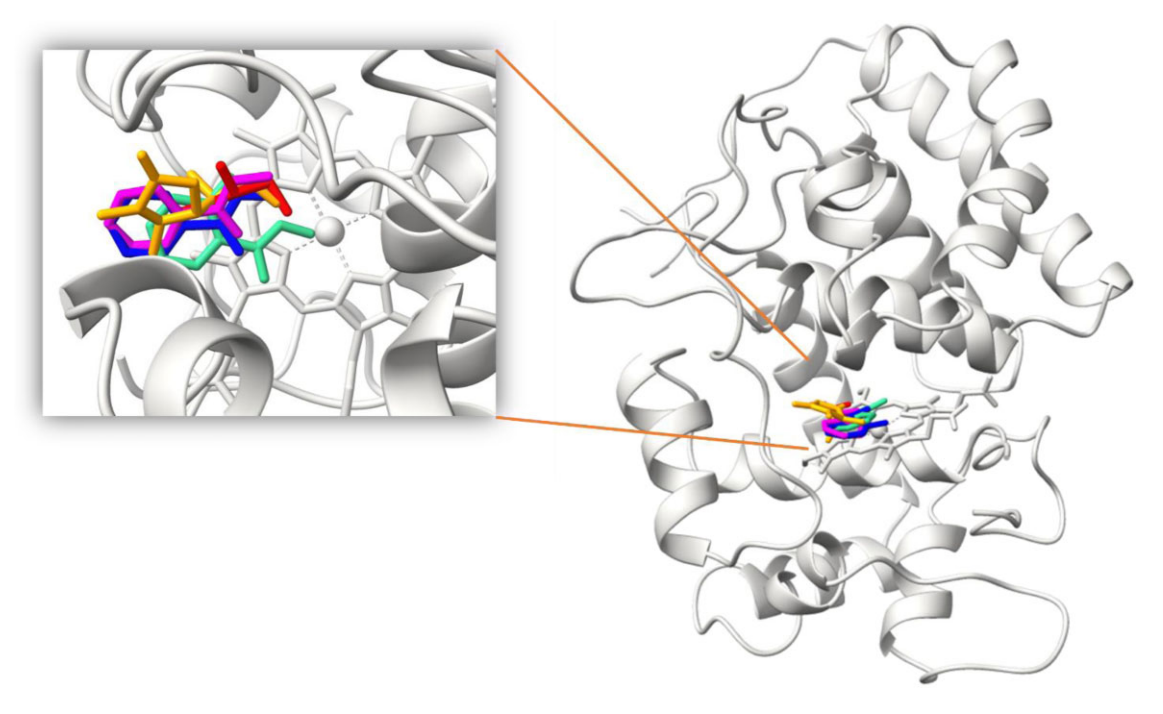


**Figure 11** Superimposition of bound ligands at the  $\delta$ -meso site. Orange, ascorbate in SbAPX; red, glycerol in SbAPX; green, SHA from rsAPX (PDBID: 1V0H); blue, SHA from ARP (PDBID: 1CK6); pink, benzohydroxamic acid from HRP (PDBID: 2ATJ). Figures were produced using the Chimera package (UCSF, NIH P41 RR-01081).

(Figure 9). Mutating the critical residue for ascorbate-binding at the  $\gamma$ -heme edge site, Arg-172, drastically reduced the ascorbate oxidation activity, indicating the surface-bound ascorbate cannot participate in the reaction unless there is an ascorbate bound at the  $\gamma$ -heme edge site.

The cumulative evidence, including ours, presented here, suggests that small organic molecules bound at the  $\delta$ -meso site can be radicalized directly or indirectly through Trp-41, His-42, Arg-38, and hydrogen-bonding water molecules. Supporting this further, mutation of the critical residue for ascorbate-binding at  $\gamma$ -heme edge site, Arg-172, was able to maintain  $\sim$ 40% of H<sub>2</sub>O<sub>2</sub>-dependent polymerization reaction (Table 2).

#### Conclusion

This study characterized the substrate-binding pockets and the plausible catalytic reaction mechanism of a monocot APX. Our study identified four binding pockets of ascorbate in SbAPX, its neutralization of  $H_2O_2$ , and ascorbate turned into bicyclic DHA at the  $\gamma$ -heme edge site. Using the  $\delta$ -meso site, SbAPX can effectively polymerize several phenyl-propanoid intermediates in the monolignol pathway in the presence  $H_2O_2$ . We were able to reproduce the 3-hydroxylation of p-coumarate in the presence of ascorbate and  $H_2O_2$  (Barros et al., 2019) and in the presence of dihydroxy-fumarate (Halliwell, 1977). However, most of the produced caffeic acid was from a nonenzymatic reaction and, thus, hydroxylation by SbAPX might be negligible.

Although the exact mechanism for translocation of mitochondrial PtomtAPX to the cell wall (Zhang et al., 2022) is not clear, there is a possibility that SbAPX could also be translocated to the cell wall during the early stages of secondary cell wall formation and xylem development. Therefore, APX, which is only known to be found in plants, algae, and photosynthetic protists, may not only remove stressgenerated  $\rm H_2O_2$  with ascorbates, but may potentially also use the same  $\rm H_2O_2$  for fortifying cell walls via oxidative polymerization of phenylpropanoids in response to stress. The substitution of amino acids within the substrate-binding region of APX could potentially lead to changes in substrate affinity and result in the diversification of its function.

#### Materials and methods

#### Recombinant enzyme expression and purification

The sorghum (*S. bicolor*) SbAPX cDNA sequence was cloned into vector pET-30a(+) (MilliporeSigma, St. Louis, MO) with N-terminal 6×His-tag for heterologous expression. The vector was introduced into *E. coli* Rosetta 2(DE3) cells via transformation. Site-directed mutagenesis for R38L, W41F, H42A, and R172A was accomplished by PCR using the primers designed by Agilent Quickchange Primer Design (https://www.agilent.com/store/primerDesignProgram.jsp). The corresponding primers are listed in Supplemental Table S2. Three-liter Luria-Bertani (LB) medium complemented with 25  $\mu$ g mL<sup>-1</sup> chloramphenicol and 50  $\mu$ g mL<sup>-1</sup> kanamycin was inoculated with 20 mL from an overnight culture. The cells were grown at 37 °C until the culture reached OD<sub>600</sub> 0.8, and IPTG was added to a final concentration of 2 mM. After being induced for 4–5 h, the cells were harvested by

centrifugation at 8,000 × g for 10 min at 4 °C. The cells were resuspended in buffer A (50 mM KP<sub>i</sub>, pH 8, 300 mM NaCl) and sonicated on ice for 30 min. (Model 450 sonicator; Branson Ultrasonics, Danbury, CT) to release soluble protein. The cell debris was removed by centrifugation at  $37,000 \times g$ for 1 h. The clear lysate was loaded on a nickel-NTA column (Qiagen, Germantown, MD) and washed with three column volumes of Buffer A. the column was then washed by three column volumes of Buffer B (50 mM Kpi, pH 6, 300 mM NaCl, 10% (v/v) glycerol) followed by two column volumes Buffer B containing 20 mM imidazole. SbAPX was eluted with Buffer B containing 200 mM imidazole. Wild-type SbAPX was naturally folded with heme during the expression, while mutant versions were not. Thus, bovine heme was dissolved into a NaOH solution and added to buffer solutions containing the mutant versions of protein. During the purification, the His-tag was spontaneously cleaved, which could be due to a thrombin site between the His-tag and SbAPX. The protein was concentrated, buffer-exchanged against 5 mM potassium phosphate buffer pH 6.8, and loaded onto a hydroxyapatite column. SbAPX was eluted by a linear gradient of potassium phosphate pH 6.8, ranging in concentration from 5 to 25 mM, and the fractions with ratio OD<sub>404</sub>: OD<sub>281</sub> > 2 were concentrated to 1 mL by using an Amicon 8050 ultrafiltration cell with a 10-kDa cutoff membrane (EMDMillipore, St. Louis, MO). The concentrate was loaded onto a column containing Superdex<sup>TM</sup> 200 Increase 10/300 GL for further purification. During the purification, a 5-kD fragment was removed from the original recombinant APX. This truncated protein was loaded on a Ni-NTA column and was collected in the flow-through, which indicated that the truncation resulted in the loss of the N-terminal His-tag. The SbAPX without His-tag was buffer-exchanged against 20 mM Tris, pH 7.5, 50 mM NaCl (Buffer C).

NMR study of H<sub>2</sub>O<sub>2</sub>-dependent oxidation of ascorbate The method followed a previous study (Kurata and Nishikawa, 2000) with some modifications. Ascorbate was dissolved in phosphate buffer (pH 7.5) in 95% (v/v) D<sub>2</sub>O and 5% (v/v) H<sub>2</sub>O with a final concentration of 10 mg dL<sup>-1</sup> to mimic physiological concentration (10-30 mg dL<sup>-1</sup>). 0.005% (v/v) of methanol was added as an internal standard for the chemical shift and integration. A <sup>1</sup>H NMR was taken for 1 mL of ascorbate solution prior to the addition of SbAPX and H<sub>2</sub>O<sub>2</sub> at 4°C. After adding 30 nM SbAPX and 2 mM H<sub>2</sub>O<sub>2</sub>, a series of <sup>1</sup>H NMR was taken up to 40 min after the reaction. 'H NMR spectra were recorded using the PRESAT pulse sequence on a Varian DD2 600 MHz NMR spectrometer, equipped with a broad banded autotuning probe (OneProbe), with a saturation frequency of -219.0 Hz (4.64 ppm), saturation power equal to 8 dB. The spectral width was 9615.4 Hz, acquisition time of 1.704 s, using 16,384 complex points, a 90° pulse of 8.90 us, and a relaxation delay of 3 s. Time course kinetic data were collected using an array function, such that 20 spectra were collected at intervals of 124 s with a 1 s delay between acquisitions. 32 scans were recorded for each

spectrum in the array. Data were processed using an exponentially weighted Fourier transform (line broadening of 2 Hz).

#### Crystallization and structure determination

Prior to crystallization, the SbAPX was concentrated to 20 mg mL<sup>-1</sup> by using an Amicon 8050 ultrafiltration cell with a 10-kDa cutoff membrane (EMDMillipore, St. Louis, MO). A commercial crystallization kit, Crystal screen HT (Hampton, Aliso Viejo, CA), was used for crystal screening through the sitting-drop, vapor-diffusion method by Crystal Phoenix (Art Robbins Instruments, Sunnyvale, CA). The initial crystal appeared in the condition B5 (0.2 M Li<sub>2</sub>SO<sub>4</sub>, 0.1 M Tris, pH 8.5%, and 30% (w/v) PEG 4000) at 4 °C. Then the larger crystals were reproduced by the sitting-drop vapor-diffusion method with the same solution. Small crystals appeared in two days. The one-ascorbate structure was obtained by soaking apo crystals in cryoprotectant containing 1 mM ascorbate for 1 min, whereas the four-ascorbate structure was obtained by soaking apo crystal in cryoprotectant containing 1 mM ascorbate for 10 min. The bicyclic hemiketal complex crystal was obtained by soaking with 50 mM ascorbate and 50 mM H<sub>2</sub>O<sub>2</sub> for 3 min. Structures containing compound II and compound III were obtained by soaking apo crystals in cryoprotectant containing 100 mM H<sub>2</sub>O<sub>2</sub> for 1 min. All crystals except for compound III were collected with 1 s per frame for 180°; compound III crystals were exposed for 0.2 s for 180°. All the statistics of deposited structures were listed in Supplemental Table S1.

#### Determination of oxidation products of SbAPX

The p-coumarate-3-hydroxylation reaction was conducted as described for recombinant APX reaction (Barros et al., 2019). For comparison of the nonenzymatic and enzymatic C3H reactions, a 600 µL reaction mixture contained 75 mM potassium phosphate buffer (pH 6), 10 mM H<sub>2</sub>O<sub>2</sub>, 4 mM sodium ascorbate, and 1 mM p-coumaric acid. For the enzymatic reaction, 150 nM SbAPX was added. The reaction was shaken at 200 rpm at 30 °C. At 0, 30, 60, and 120 min, 90 μL of reaction mixture was removed and immediately mixed with 10 µL glacial acetic acid. The H<sub>2</sub>O<sub>2</sub>-dependent reaction was conducted in 1 mL 50 mM potassium phosphate buffer, pH 7.5 containing 100 μM p-coumarate, cinnamate, caffeate, ferulate, sinapate, coniferyl alcohol, coniferyl aldehyde or tyrosine, 1 mM H<sub>2</sub>O<sub>2</sub>, and 5 µM of purified SbAPX or mutant versions. The kinetic assay for H<sub>2</sub>O<sub>2</sub>-dependent oxidation of p-coumarate was conducted with 10 to 500 μM p-coumarate. The reaction mixture was incubated at room temperature for 10 min and quenched by 30% (v/v) glacial acetic acid prior to injection to HPLC. The reaction mixture was injected onto a Luna® 5 μm C18 column and the product was monitored by HPLC (Hitachi Elite LaChrom L-2100; Hitachi High-Tech, Schaumburg, IL) operating at a flow rate of 1 mL min<sup>-1</sup>, with a gradient of solvent A (0.1% (v/v) trifluoroacetic acid in deionized water) and solvent B (100% acetonitrile) varying from 95% A and 5% B to 0% A and 100% B over a period of 30 min. Products were quantified by detection at 320 nm using the Hitachi Elite LaChrom L-2400 detector. All experiments were performed in triplicate. The kinetic data were analyzed using Michaelis—Menten equations. The reaction products of SbAPX for most other phenylpropanoid intermediates could not be analyzed due to substantially increased viscosity under the identical condition and high backpressure buildup right after HPLC-injection, indicating generation of larger polymer products.

### ESI-MS for the product of H<sub>2</sub>O<sub>2</sub>-dependent oxidation of p-coumarate by SbAPX

To accumulate the product peaks for MS analysis, a 10 mL p-coumarate H<sub>2</sub>O<sub>2</sub> dependent oxidation reaction containing 50 mM potassium phosphate buffer, pH 7.5 containing 100  $\mu$ M p-coumarate, 1 mM H<sub>2</sub>O<sub>2</sub>, and 5  $\mu$ M of purified SbAPX was incubated at room temperature for 30 min before lyophilization. The lyophilized reaction mixture was loaded on a C18 prep column (Waters, Milford, MA), and the individual eluted compounds were collected, lyophilized, and resuspended in 0.1% (v/v) formic acid in acetonitrile. The samples were infused at 10 µl/min into the Thermo Q-Exactive-HF mass spectrometer by Proteomics and Metabolomics Core Facility at University of Nebraska-Lincoln (https://biotech. unl.edu/proteomics-and-metabolomics). Mass spectra were acquired using negative and positive ion modes using a mass range of m/z 100-100 at a resolution of 120,000 for the MS1 peptide measurements. MS2 spectra were acquired by HCD with normalized collision energy set manually depending on each of the peaks selected. Analyst software (version 1.6.3) was used to control sample acquisition and data analysis. The ESI source operation parameters were as follows: source temperature at 500°C; ion spray voltage at 5,500 for positive, and -4,500 for negative ion mode; ion source gas 1 at 50; ion source gas 2 at 50; curtain gas at 20 psi; collision gas at medium.

#### Dihydroxyfumarate

The hydroxylation of *p*-coumarate was conducted in 1 mL 50 mM sodium phosphate buffer, pH 6 containing 100  $\mu$ M *p*-coumarate, 1 mM dihydroxyfumarate, and 5  $\mu$ M of purified SbAPX. The control reaction contained the same components without SbAPX. Both mixtures were incubated at room temperature for 2 h prior to injection to HPLC.

MALDI-TOF MS for determination of dihydroxyfumarate reaction: The reaction was run on a C18 prep column (Waters, Milford, MA), and the product peak was collected and lyophilized prior to MS analysis. The lyophilized powder was dissolved in 50% (v/v) acetonitrile. The matrix, α-cyano-4-hydroxycinnamic acid, CHCA (Sigma-Aldrich, St. Louis, MO) was prepared as a solution of 10 mg mL<sup>-1</sup> in 50% (v/v) water/acetonitrile with 0.1% (v/v) TFA. The matrix solution was mixed 1:1 with the product peak solution, applied to the sample plate, and dried. Spectra were collected using a 4,800 MALDI TOF/TOF Analyzer (Applied Biosystems, Waltham, MA), using the data collection programs in negative mode for MS spectra.

#### Steady-state kinetics of SbAPX

Kinetic assays of SbAPX with ascorbate were performed with 1 mM  $\rm H_2O_2$  in 50 mM potassium phosphate buffer, pH 7.0 at room temperature in a GENESYS<sup>TM</sup> 10S UV-Vis Spectrophotometer (Thermo Scientific, Waltham, MA) spectrophotometer. The concentration of ascorbate varied from 10 to 1200  $\mu$ M and the final concentration of SbAPX was 15 nM. The reaction was initiated by adding SbAPX. The activity was calculated by the rate of disappearance of ascorbate ( $\epsilon$ =2.8 mM $^{-1}$ ·cm $^{-1}$ ) at 290 nm during the first minute (Nakano and Asada, 1981). The corresponding activity for mutants was measured with the same setup above.

#### Molecular docking of SbAPX

Ascorbate, *p*-coumarate, salicylhydroxamate, glycerol, and the phenylpropanoid intermediates of the monolignol pathway were docked into the entire SbAPX by AutoDock Vina (Trott and Olson, 2010) for global search; ligands and grids were prepared for docking using AutoDock Tools (Morris et al., 2009). The grid box was 100×100×100 Å. The exhaustiveness was set to 25 due to the large grid box.

#### **Accession numbers**

Sequence data from this publication can be found in the EMBL/GenBank data libraries under accession number XP\_002468053.1.

#### Supplemental data

The following materials are available in the online version of this article.

**Supplemental Table S1.** Crystallography statistics of SbAPX structures.

**Supplemental Table S2.** Primer list of site-directed mutagenesis.

**Supplemental Figure S1**. Mass spectroscopy spectrum of SbAPX oxidation products.

**Supplemental Figure S2.** Overall structure of SbAPX with 1-minute soak in 1 mM ascorbate without H<sub>2</sub>O<sub>2</sub> (8DJS).

**Supplemental Figure S3.** Sequence alignment of ascorbate peroxidases.

Supplemental Figure S4. Surface analysis of SbAPX.

#### **Acknowledgments**

We thank the Proteomics & Metabolomics Facility (RRID: SCR\_021314), Nebraska Center for Biotechnology at the University of Nebraska-Lincoln for the ESI-MS mass spectrometry analysis. The facility and instrumentation are supported by the Nebraska Research Initiative. We thank Dr. Munske R. Gerhard for the MALDI/TOF MS analyses of the APX products. We also thank Emily Savoy for technical assistance using HPLC for the kinetic assays and Dr. William Hiscox for technical assistance with the NMR study.

#### Data availability

The structure discussed in this manuscript can be found at www.rcsb.org deposited under the corresponding PDB IDs: 8DIR, 8DIS, 8DIT, 8DIU, 8DIW, and 8DIX.

#### **Funding**

Original research was supported by grant from NSF (CHE-1804699, MCB-2043248) and Murdock Charitable Trust (C.H.K.). This research used resources of the Advanced Light Source (beamline 5.0.1, beamline 5.0.2, and beamline 8.2.2), which is a DOE Office of Science User Facility under contract no. DE-AC02-05CH11231. S.E.S. acknowledges support from USDA-ARS United States Department of Agriculture, Agriculture Research Service Project 3042-21220-033-000-D.

Conflict of interest statement. The authors declare no conflict of interest exists in the conducted work.

#### References

- Barros J, Escamilla-Trevino L, Song LH, Rao XL, Serrani-Yarce JC, Palacios MD, Engle N, Choudhury FK, Tschaplinski TJ, Venables BJ, et al. (2019) 4-Coumarate 3-hydroxylase in the lignin biosynthesis pathway is a cytosolic ascorbate peroxidase. Nat Commun 10(1): 1994
- Carroll V, Truillet C, Shen B, Flavell R, Shao X, Evans M, VanBrocklin H, Scott P, Chin F, Wilson D (2016) [11 C] ascorbic and [11 C] dehydroascorbic acid, an endogenous redox pair for sensing reactive oxygen species using positron emission tomography. Chem Commun 52(27): 4888–4890
- Charles SA, Halliwell B (1980) Effect of hydrogen peroxide on spinach (Spinacia oleracea) chloroplast fructose bisphosphatase. Biochem J 189(2): 373–376
- Copeland RA (2000) Enzymes: a practical introduction to structure, mechanism, and data analysis. John Wiley & Sons, Hoboken, NJ.
- Fawal N, Li Q, Savelli B, Brette M, Passaia G, Fabre M, Mathé C, Dunand C (2012) Peroxibase: a database for large-scale evolutionary analysis of peroxidases. Nucleic Acids Res 41(D1): D441-D444
- Francoz E, Ranocha P, Nguyen-Kim H, Jamet E, Burlat V, Dunand C (2015) Roles of cell wall peroxidases in plant development. Phytochemistry **112**(1): 15–21
- Halliwell B (1977) Generation of hydrogen peroxide, superoxide and hydroxyl radicals during the oxidation of dihydroxyfumaric acid by peroxidase. Biochem J 163(3): 441–448
- **Halliwell B, Ahluwalia S** (1976) Hydroxylation of *p*-coumaric acid by horseradish peroxidase. The role of superoxide and hydroxyl radicals. Biochem J **153**(3): 513–518
- **Harkin JM, Obst JR** (1973) Lignification in trees: indication of exclusive peroxidase participation. Science **180**(4083): 296–298
- Heering HA, Jansen MA, Thorneley RN, Smulevich G (2001) Cationic ascorbate peroxidase isoenzyme II from tea: structural insights into the heme pocket of a unique hybrid peroxidase. Biochemistry 40(34): 10360–10370
- **Higuchi T** (1985) Biosynthesis Biodegrad Wood Compon. Academic Press Inc., Orlando, FL, pp 141–160
- Hill AP, Modi S, Sutcliffe MJ, Turner DD, Gilfoyle DJ, Smith AT, Tam BM, Lloyd E (1997) Chemical, spectroscopic and structural investigation of the substrate-binding site in ascorbate peroxidase. Eur J Biochem 248(2): 347–354

- Hiner AN, Raven EL, Thorneley RN, García-Cánovas F, Rodríguez-López JN (2002) Mechanisms of compound I formation in heme peroxidases. J Inorg Biochem 91(1): 27–34
- Holm L, Rosenstrom P (2010) Dali server: conservation mapping in 3D. Nucleic Acids Res 38(suppl\_2): W545–W549
- Jensen G, Bunte S, Warshel A, Goodin D (1998) Energetics of cation radical formation at the proximal active site tryptophan of cytochrome c peroxidase and ascorbate peroxidase. J Phys Chem B 102-(42): 8221–8228
- **Kaiser W** (1976) The effect of hydrogen peroxide on CO<sub>2</sub> fixation of isolated intact chloroplasts. Biochim Biophys Acta **440**(3): 476–482
- Kjalke M, Andersen MB, Schneider P, Christensen B, Schülein M, Welinder KG (1992) Comparison of structure and activities of peroxidases from Coprinus cinereus, Coprinus macrorhizus and Arthromyces ramosus. Biochim Biophys Acta 1120(3): 248–256
- Krissinel E, Henrick K (2007) Inference of macromolecular assemblies from crystalline state. J Mol Biol 372(3): 774–797
- Kurata T, Nishikawa Y (2000) Chemical characteristics of dehydro-L-ascorbic acid. Biosci Biotechnol Biochem 64(8): 1651–1655
- Kwon H, Basran J, Casadei CM, Fielding AJ, Schrader TE, Ostermann A, Devos JM, Aller P, Blakeley MP, Moody PCE, et al. (2016) Direct visualization of a Fe(IV)-OH intermediate in a heme enzyme. Nat Commun 7(1): 13445
- Kwon H, Basran J, Devos JM, Suardíaz R, van der Kamp MW, Mulholland AJ, Schrader TE, Ostermann A, Blakeley MP, Moody PCE, et al. (2020) Visualizing the protons in a metalloenzyme electron proton transfer pathway. Proc Natl Acad Sci USA 117(12): 6484–6490
- **Lad L, Mewies M, Raven EL** (2002) Substrate binding and catalytic mechanism in ascorbate peroxidase: evidence for two ascorbate binding sites. Biochemistry **41**(46): 13774–13781
- Lazzarotto F, Menguer PK, Del-Bem L-E, Zámocký M, Margis-Pinheiro M (2021) Ascorbate peroxidase neofunctionalization at the origin of APX-R and APX-L: evidence from basal archaeplastida. Antioxidants 10(4): 597
- Ledray AP, Krest CM, Yosca TH, Mittra K, Green MT (2020)
  Ascorbate peroxidase compound II is an iron (IV) oxo species. J
  Am Chem Soc 142(48): 20419–20425
- Lee Y, Rubio MC, Alassimone J, Geldner N (2013) A mechanism for localized lignin deposition in the endodermis. Cell **153**(2): 402–412
- Li Y, Kajita S, Kawai S, Katayama Y, Morohoshi N (2003) Down-regulation of an anionic peroxidase in transgenic aspen and its effect on lignin characteristics. J Plant Res 116(3): 175–182
- Macdonald IK, Badyal SK, Ghamsari L, Moody PCE, Raven EL (2006) Interaction of ascorbate peroxidase with substrates: a mechanistic and structural analysis. Biochemistry 45(25): 7808–7817
- Makita Y, Shimada S, Kawashima M, Kondou-Kuriyama T, Toyoda T, Matsui M (2015) MOROKOSHI: transcriptome database in Sorghum bicolor. Plant Cell Physiol **56**(1): e6
- Marjamaa K, Kukkola EM, Fagerstedt KV (2009) The role of xylem class III peroxidases in lignification. J Exp Bot 60(2): 367–376
- Mittler R, Vanderauwera S, Gollery M, Van Breusegem F (2004)
  Reactive oxygen gene network of plants. Trends Plant Sci 9(10): 490–498
- Miyake C, Asada K (1992) Thylakoid-bound ascorbate peroxidase in spinach chloroplasts and photoreduction of its primary oxidation product monodehydroascorbate radicals in thylakoids. Plant Cell Physiol 33(5): 541–553
- Moody PC, Raven EL (2018) The nature and reactivity of ferryl heme in compounds I and II. Acc Chem Res 51(2): 427–435
- Morris GM, Huey R, Lindstrom W, Sanner MF, Belew RK, Goodsell DS, Olson AJ (2009) Autodock4 and AutoDockTools4: automated docking with selective receptor flexibility. J Comput Chem 30(16): 2785–2791
- Moural TW, Lewis KM, Barnaba C, Zhu F, Palmer NA, Sarath G, Scully ED, Jones JP, Sattler SE, Kang C (2017) Characterization of class III peroxidases from switchgrass. Plant Physiol 173(1): 417–433

- Nakano Y, Asada K (1981) Hydrogen peroxide is scavenged by ascorbate-specific peroxidase in spinach chloroplasts. Plant Cell Physiol 22(5): 867-880
- Náray-Szabó G (1997) Electrostatic modulation of electron transfer in the active site of heme peroxidases. J Biol Inorg Chem 2(1): 135-138
- Pandey S, Fartyal D, Agarwal A, Shukla T, James D, Kaul T, Negi YK, Arora S, Reddy MK (2017) Abiotic stress tolerance in plants: myriad roles of ascorbate peroxidase. Front Plant Sci 8(1): 581
- Pappa H, Patterson WR, Poulos TL (1996) The homologous tryptophan critical for cytochrome c peroxidase function is not essential for ascorbate peroxidase activity. J Biol Inorg Chem 1(1): 61-66
- Paterson AH, Bowers JE, Bruggmann R, Dubchak I, Grimwood J, Gundlach H, Haberer G, Hellsten U, Mitros T, Poliakov A (2009) The Sorghum bicolor genome and the diversification of grasses. Nature 457(7229): 551-556
- Patterson WR, Poulos TL (1995) Crystal structure of recombinant pea cytosolic ascorbate peroxidase. Biochemistry 34(13): 4331-4341
- Patterson WR, Poulos TL, Goodin DB (1995) Identification of a porphyrin.pi. Cation radical in ascorbate peroxidase compound I. Biochemistry 34(13): 4342-4345
- Pfeilsticker K, Marx F, Bockisch M (1975) Zur struktur der dehydroascorbinsäure in wäsriger lösung. Carbohydr Res 45(1): 269-274
- Polle A, Wieser G, Havranek W (1995) Quantification of ozone influx and apoplastic ascorbate content in needles of Norway spruce trees (Picea abies L., Karst) at high altitude. Plant Cell Environ 18(6): 681-688
- Prinz H (2010) Hill coefficients, dose-response curves and allosteric mechanisms. J Chem Biol 3(1): 37-44
- Raven EL (2000) Peroxidase-catalyzed oxidation of ascorbate. Structural, spectroscopic and mechanistic correlations in ascorbate peroxidase. Subcell Biochem 35(1): 317-349
- Saxena S, Joshi P, Grimm B, Arora S (2011) Alleviation of ultraviolet-C-induced oxidative damage through overexpression of cytosolic ascorbate peroxidase. Biologia 66(6): 1052-1059
- Shakoor N, Nair R, Crasta O, Morris G, Feltus A, Kresovich S (2014) A Sorghum bicolorexpression atlas reveals dynamic genotype-specific expression profiles for vegetative tissues of grain, sweet and bioenergy sorghums. BMC Plant Biol 14(1): 1-15
- Sharp KH, Mewies M, Moody PC, Raven EL (2003) Crystal structure of the ascorbate peroxidase-ascorbate complex. Nat Struct Mol Biol 10(4): 303-307
- Sharp KH, Moody PC, Brown KA, Raven EL (2004) Crystal structure of the ascorbate peroxidase- salicylhydroxamic acid complex. Biochemistry 43(27): 8644-8651

- Sundaramoorthy M, Kishi K, Gold MH, Poulos TL (1994) The crystal structure of manganese peroxidase from Phanerochaete chrysosporium at 2.06-A resolution. J Biol Chem 269(52): 32759-32767
- Teixeira FK, Menezes-Benavente L, Margis R, Margis-Pinheiro M (2004) Analysis of the molecular evolutionary history of the ascorbate peroxidase gene family: inferences from the rice genome. J Mol Evol 59(6): 761-770
- Tolbert BM, Ward JB (1982) Dehydroascorbic acid. In ascorbic acid: chemistry, metabolism, and uses. Am Chem Soc 200(1): 101-123
- Trott O, Olson AJ (2010) Autodock vina: improving the speed and accuracy of docking with a new scoring function, efficient optimization, and multithreading. J Comput Chem 31(2): 455-461
- Van Breusegem F, Dat JF (2006) Reactive oxygen species in plant cell death. Plant Physiol 141(2): 384-390
- Vanholme R, De Meester B, Ralph J, Boerjan W (2019) Lignin biosynthesis and its integration into metabolism. Curr Opin Biotechnol 56(1): 230-239
- Vera JC, Rivas CI, Fischbarg J, Golde DW (1993) Mammalian facilitative hexose transporters mediate the transport of dehydroascorbic acid. Nature 364(6432): 79-82
- Wada K, Tada T, Nakamura Y, Ishikawa T, Yabuta Y, Yoshimura K, Shigeoka S, Nishimura K (2003) Crystal structure of chloroplastic ascorbate peroxidase from tobacco plants and structural insights into its instability. J Biochem 134(2): 239-244
- Wang Y-Y, Hecker AG, Hauser BA (2014) The APX4 locus regulates seed vigor and seedling growth in Arabidopsis thaliana. Planta 239(4): 909-919
- Washko PW, Wang Y, Levine M (1993) Ascorbic acid recycling in human neutrophils. J Biol Chem 268(21): 15531-15535
- Welinder KG (1992) Superfamily of plant, fungal and bacterial peroxidases. Curr Opin Struct Biol 2(3): 388-393
- Winkler BS, Orselli SM, Rex TS (1994) The redox couple between glutathione and ascorbic acid: a chemical and physiological perspective. Free Radical Biol Med 17(4): 333-349
- Yao T, Feng K, Xie M, Barros J, Tschaplinski TJ, Tuskan GA, Muchero W, Chen J-G (2021) Phylogenetic occurrence of the phenylpropanoid pathway and lignin biosynthesis in plants. Front Plant Sci **12**(1): 704697
- Zhang J, Liu Y, Li C, Yin B, Liu X, Guo X, Zhang C, Liu D, Hwang I, Li H, et al. (2022) PtomtAPX is an autonomous lignification peroxidase during the earliest stage of secondary wall formation in Populus tomentosa carr. Nat Plants 8(7): 828-839